Endoplasmic reticulum Ca(2+) content decrease by PKA-dependent hyperphosphorylation of type 1 IP3 receptor contributes to prostate cancer cell resistance to androgen deprivation.

Benoît Boutin, Nicolas Tajeddine, Giovanni Monaco, Jordi Molgó, Didier Vertommen, Mark Rider, Jan B Parys, Geert Bultynck, Philippe Gailly

Endoplasmic reticulum Ca^{2+} content decrease by PKA-dependent hyperphosphorylation of type 1 IP3 receptor contributes to prostate cancer cell resistance to androgen deprivation

Benoît Boutin [1, †], Nicolas Tajeddine [1, †], Giovanni Monaco [2], Jordi Molgo [3], Didier Vertommen [4], Mark Rider [4], Jan B. Parys [2], Geert Bultynck [2], Philippe Gailly [1,*]

[1] Laboratory of Cell Physiology, Institute of Neuroscience, Université catholique de Louvain, Brussels, Belgium

[2] Laboratory of Molecular and Cellular Signaling, Department of Cellular and Molecular Medicine, KU Leuven, Leuven, Belgium

[3] CNRS, Institut de Neurobiologie Alfred Fessard, Laboratoire de Neurobiologie et Développement, UPR 3294, 1 Avenue de la Terrasse, bâtiments 32-33, 91198 Gif sur Yvette Cedex, France

[4] de Duve Institute, Université catholique de Louvain, Brussels, Belgium

[†] These authors contributed equally to this work.

Running title: IP3R1 phosphorylation, $[Ca^{2+}]_{ER}$ and apoptosis

Keywords: IP3R1; apoptosis; endoplasmic reticulum; prostate cancer; PKA; hormone therapy

*** Correspondence to**: Philippe Gailly, Université catholique de Louvain, Institute of Neuroscience, Laboratory of Cell Physiology, Avenue Mounier, B1.53.17, 1200 Brussels, Belgium. Phone: 32 2 764 55 42; Fax: 32 2 764 55 80; E-mail: philippe.gailly@uclouvain.be

ABSTRACT

Reference treatment of advanced prostate cancer (PCa) relies on pharmacological or surgical androgen deprivation therapy. However, it is only temporarily efficient as tumour cells inevitably adapt to the low testosterone environment and become hormone-refractory (HRPCa). We observed that androgen removal in HRPCa-derived LNCaP cells causes different alterations in their Ca^{2+} homeostasis among which a reduction of ER Ca^{2+} content. We show that the decrease in $[Ca^{2+}]_{ER}$ is due to a modest overexpression of type 1 IP3R and a 3-fold increased phosphorylation of IP3R1 on Ser-1716, a protein kinase A (PKA) consensus site, both implicated in ER Ca^{2+} leak. Accordingly, ER Ca^{2+} content was restored by siRNA-mediated down-regulation of IP3R1 or by inhibition of its phosphorylation by competition with a permeant TAT-peptide containing the Ser-1716 consensus phosphorylation sequence or by treatment with the PKA inhibitor H89. Moreover, inhibition of the IP3R1 phosphorylation by both methods sensitized the LNCaP cells to androgen deprivation-induced apoptosis. In addition, SERCA2b overexpression precluded the effect of androgen deprivation on ER Ca^{2+} store content and reduced resistance to androgen deprivation. Taken together, these results indicate that lowering the ER Ca^{2+}-store content by increasing IP3R1 levels and IP3R1 phosphorylation by PKA is a protective mechanism by which HRPCa-derived cells escape cell death in the absence of androgenic stimulation.

INTRODUCTION

Metastatic prostate cancer (PCa) is associated with a poor prognosis with a 5-year relative survival of 27% [1]. Reference treatment of metastatic PCa consists in pharmacological or surgical androgen deprivation therapy. However, androgen deprivation is only temporarily efficient. After a few months or years, the tumor inevitably relapses despite the absence of androgenic stimulation and becomes hormone-refractory (HRPCa). Effective treatment at this stage is largely limited to docetaxel-based chemotherapies conferring a median survival of only 17 to 19 months [2, 3]. Among commercially available HRPCa cell lines, only LNCaP cells harbor the androgen receptor (AR) [4].

The role of Ca^{2+} in prostate involution induced by androgen deprivation (AD) has been recognized for more than two decades [5]. Mitochondrial membrane permeabilization (MMP) constitutes a key event in apoptotic cell death [6]. At least, two mechanisms can enhance the Ca^{2+} transfer between ER and mitochondria. On the one hand, this could be related to an increase in Ca^{2+} conductance between ER and mitochondria after apoptosis induction. Indeed, it has been proposed that excessive transfer of Ca^{2+} from the ER to the mitochondria possibly through a protein complex comprising the inositol trisphosphate receptor, the glucose-regulated protein 75 and the voltage-dependent anion channel (IP3R/grp75/VDAC) [7] via MMP induction, release of intermembrane proapoptotic factors, dissipation of mitochondrial transmembrane potential ($\Delta\Psi_m$), formation of apoptosomes and subsequent cell death [8, 9]. Thus, overactivation/overexpression of one member of the IP3R/grp75/VDAC complex could enhance the sensitivity to proapoptotic agents. On the other hand, the ER-mitochondria Ca^{2+} flux might be enhanced by an increase in the electrochemical gradient e.g. subsequently to an increase in $[Ca^{2+}]_{ER}$. Indeed, antiapoptotic proteins such as Bcl-2 or Bcl-X_L decrease $[Ca^{2+}]_{ER}$ whereas proapoptotic proteins such as Bax or Bak have the opposite effect, at least in some cell systems [10]. This suggests that $[Ca^{2+}]_{ER}$ is closely related to the sensitivity to cytotoxic stimuli [11]. Increase in $[Ca^{2+}]_{ER}$ can be secondary to an increase in the ER refilling, e.g. due to an increase in SERCA activity or expression, or to a decrease in Ca^{2+} leak from

ER. In mouse embryonic fibroblasts, the group of Korsmeyer showed several years ago that IP3R1 constituted an ER Ca^{2+} leak channel, the permeability of which was modulated by a protein kinase A (PKA)-mediated phosphorylation, itself increased by Bcl-2 and decreased by Bax or Bak expression [12]. In T-lymphocytes however Bcl-2 can dock both DARPP-32 and calcineurin to the IP3R, whereby the PKA-mediated phosphorylation of the latter is antagonized, leading to decreased IP3R-mediated Ca^{2+} release [13]. Very recently, in an siRNA screen for the identification of ER Ca^{2+}-leak channels, IP3R1 channels emerged as one of the most prominent Ca^{2+}-transport systems implicated in ER Ca^{2+} leak [14].

In the present study, we show that AD decreases $[Ca^{2+}]_{ER}$ in LNCaP cells and suggest that this is mediated by a phosphorylation-dependent increase in IP3R1 permeability. Inhibition of IP3R1 phosphorylation restores LNCaP cells sensitivity to AD and could be a novel therapeutic target for the treatment of HRPCa.

RESULTS

Androgen deprivation alters intracellular Ca^{2+} homeostasis

In order to study the effects of AD on $[Ca^{2+}]_c$ and on $[Ca^{2+}]_{ER}$, we measured $[Ca^{2+}]_c$ in LNCaP cells cultured in the absence or in the presence of synthetic androgen R1881 for 48 h. Fura-2 loaded cells were treated with the SERCA inhibitor thapsigargin in the absence of external Ca^{2+} and then, Ca^{2+} was reintroduced in the external medium to evaluate the amplitude of store-operated Ca^{2+} entry (SOCE). We observed that AD had no effect on $[Ca^{2+}]_c$ but reduced by about 40% the amount of thapsigargin-induced Ca^{2+} release, suggesting a decrease of the ER Ca^{2+} store content. SOCE was also decreased after AD (Fig. 1A and B). Interestingly, treatment of the cells with the AR specific inhibitor bicalutamide (50 μM) for 48 hours also decreased releasable Ca^{2+} from the ER (data not shown). We also observed that basal influx of Ca^{2+} through the plasma membrane as measured by the Mn^{2+}-induced Fura-2 quenching technique was diminished after androgen removal (Fig. 1C).

We therefore tried to decipher the mechanisms underlying these modifications and measured the expression of a series of proteins possibly involved in Ca^{2+} homeostasis (Ca^{2+} pumps, channels and buffers). AD induced a strong decrease in TRPM8 expression and a more than 2-fold increase in IP3R1 expression at the mRNA level (Fig. 2). Previous studies have shown that the expression of the Ca^{2+} channel TRPM8 is highly dependent on the presence of androgens and is overexpressed in prostate cancer cells [15, 16]. Its repression after androgen removal might therefore explain alterations in Ca^{2+} homeostasis. IP3R1 beside its well-known role in agonist-induced Ca^{2+} signaling, might also function as an ER Ca^{2+} leak channel [12, 17], thereby controlling resting $[Ca^{2+}]_{ER}$. Importantly, its activity has been reported to be phosphorylation-dependent [18].

Involvement of TRPM8 in Ca^{2+} homeostasis alterations induced by AD

Given the importance of AD on TRPM8 expression, we tried to mimic this effect by depleting TRPM8 in LNCaP cells using specific siRNA. The silencing of TRPM8 was proved by RT-qPCR (Fig. 3A) and was correlated with a significant decrease of basal influx of Ca^{2+} (Fig. 3C). This indicates that the channel is expressed, at least partially, at the plasma membrane and that the decrease of its expression due to AD could be responsible for basal Ca^{2+} influx reduction. However, we did not observe any subsequent decrease in $[Ca^{2+}]_c$, in thapsigargin-evoked Ca^{2+} release or in SOCE (Fig. 3B).

Involvement of IP3R1 in Ca^{2+} homeostasis alterations induced by AD

It has been suggested that IP3R1 could control resting $[Ca^{2+}]_{ER}$ [12, 14]. After AD treatment in LNCaP cells, we observed a modest increase in the amount of IP3R1 protein (Fig. 4A and B) and a dramatic increase in IP3R1 phosphorylation on the PKA consensus site Ser-1716 (equivalent to Ser-1756 in the rat IP3R1 amino acid sequence). Incidentally, IP3R2 was not expressed in LNCaP cells [19] and expression of IP3R3 mRNA was not modified by AD (Fig. 2).

In order to evaluate the effects of IP3R1 phosphorylation and expression on $[Ca^{2+}]_{ER}$, we first measured the Ca^{2+} content in the ER after inhibition of PKA-mediated IP3R1 phosphorylation. As also performed in Fig. 1, we tried to evaluate $[Ca^{2+}]_{ER}$ after thapsigargin treatment. However, we observed that acute inhibition (5 minutes pretreatement) of IP3R by xestospongin B decreased by itself the amount of releasable Ca^{2+} (Fig. 5A). This suggested that IP3R is the Ca^{2+} leak channel in thapsigargin-induced ER depletion. Since we were interested in the permeability of IP3R, a procedure using thapsigargin to evaluate $[Ca^{2+}]_{ER}$ was obviously inadequate. We then decided to use ionomycin to permeabilize the ER membrane and measure releasable Ca^{2+} independently of the IP3R-mediated leak. We observed that the ionomycin-induced Ca^{2+} release was decreased by AD (Fig. 5E and F), confirming the results obtained with thapsigargin (Fig. 1B). We then interfered with IP3R1 phosphorylation by using a cell-permeable TAT-peptide (TAT-IP3R1^{S1716}) containing the Ser-1716 consensus phosphorylation sequence. AD-induced phosphorylation of IP3R1 was abolished after treatment with 80 µM TAT-IP3R1^{S1716} (Fig. 5B and C). As Ser-1716 is known to be phosphorylated by PKA [20, 21], we treated LNCaP cells with H89, a selective inhibitor of this kinase. We observed that 10 µM H89 treatment strongly reduced IP3R1 phosphorylation (Fig. 5B and 5D). This effect was stronger than that observed with TAT-IP3R1^{S1716} treatment and occurred even in the presence of androgen. In the presence of 80 µM TAT-IP3R1^{S1716}, the effect of AD on ionomycin-induced Ca^{2+} release was abolished (Fig. 5E). Inhibition of PKA by H89 strongly increased $[Ca^{2+}]_{ER}$ and also inhibited AD-induced decrease in $[Ca^{2+}]_{ER}$ (Fig. 5F).

Involvement of IP3R1 phosphorylation in the resistance to AD

The results presented above suggest that the decrease in $[Ca^{2+}]_{ER}$ is due to an increase of the amount of IP3R1 phosphorylated on its serine 1716 residue consecutively to AD. We therefore investigated whether this process was involved in the resistance of LNCaP cells to AD. LNCaP cells were treated for 72h with 80 µM TAT-IP3R1^{S1716} in the presence or in the absence of androgen. Simultaneous fluorimetric detection of mitochondrial membrane potential ($\Delta\Psi_m$) dissipation and

plasma membrane permeabilization, two markers associated with cell death, showed that TAT-IP3R1^{S1716} strongly sensitized LNCaP cells to AD (Fig. 6A and B). TAT-IP3R1^{S1716} did however not exert any effect on cell death in the presence of androgen.

Additionally, we observed that 10 μM H89 also restored AD-dependent cell death but did not affect cell viability in the presence of androgen (Fig. 6C and D). Its effect on AD-dependent cell death was strongly diminished by adding 0.5 μM thapsigargin during the last 24 hours of AD treatment. This suggests that the inhibition of PKA by H89 exerts its effect on cell death by modulating $[Ca^{2+}]_{ER}$.

To confirm the role of Ca^{2+} store in the resistance to AD, we partially prevented AD-induced Ca^{2+} store depletion by overexpressing SERCA2b, the isoform the most ubiquitously expressed in non-muscle tissues (Fig. 7A) and measured the effects of such $[Ca^{2+}]_{ER}$ stabilization on cell survival. We observed that SERCA2b overexpression increased the proportion of apoptotic cells after AD treatment proving ER Ca^{2+} store control on LNCaP sensitivity to AD (Fig. 7B).

Effects of IP3R1 phosphorylation on autophagy

We previously showed that AD induces autophagy in LNCaP cells and that genetic or pharmacological inhibition of autophagy also restores AD-dependent cell death [22]. Furthermore, IP3Rs and downstream Ca^{2+} signaling have been implicated in mTOR-controlled autophagy [23, 24]. We therefore studied here whether AD-induced $[Ca^{2+}]_{ER}$ modulation was involved in autophagy.

Upon autophagy induction, the LC3-I protein is modified into the lipidated form, LC3-II. This latter is associated with autophagosomes and its detection is routinely used to monitor autophagy [25]. We observed that LC3-II levels declined after AD (Fig. 8A and B). To distinguish whether this observation was due to a decrease in the on-rate of autophagic LC3-II formation or an increase in the off-rate of, the lysosomal LC3-II degradation, we used a combination of E64d and pepstatin A to inhibit lysosomal function and block LC3-II degradation. The use of inhibitors revealed that

LC3-II was increased, demonstrating that AD promotes autophagy at the level of the autophagosomal/lysosomal fusion and/or degradation events. Together, these observations confirm our previous study showing that AD increases autophagic rate in LNCaP cells [22].

H89 treatment did not preclude AD-induced LC3-II degradation, suggesting that phosphorylation of IP3R1 is not responsible for the AD-induced autophagy flux at the level of autophagosomes/lysosomes (Fig. 8A and B). These results were corroborated by detection of another biochemical sign of autophagy, namely the redistribution of GFP-LC3 fusion protein from a ubiquitous, diffuse pattern towards autophagosomes, which became visible as cytoplasmic puncta, independently of the presence of H89 (Fig. 8C).

Consistent with these findings, genetic inhibition of autophagy by siRNA-mediated depletion of the essential autophagy gene product Atg5 did not modify AD-induced decrease of the thapsigargin-releasable pool of Ca^{2+} (Fig. 8D). This suggests that the effects of AD on Ca^{2+} stores were not due to an autophagic degradation of ER membranes or ER proteins involved in intracellular Ca^{2+} handling in addition to the control of IP3R1 permeability.

DISCUSSION

Several reports have demonstrated the role of $[Ca^{2+}]_{ER}$ in the resistance to proapoptotic stimuli and increased proliferation, two major hallmarks of cancer cells [26, 27]. In LNCaP cells, AD for 96h has been shown to induce neuroendocrine differentiation associated with a reduction in $[Ca^{2+}]_{ER}$. This observation was attributed to a decreased expression of SERCA2b and of the luminal Ca^{2+}-binding/storage chaperone protein calreticulin and was correlated with a decrease in sensitivity to thapsigargin and TNF-α [28]. In our experiments, we confirmed the decrease in $[Ca^{2+}]_{ER}$ after AD but expression levels of SERCA2b and calreticulin were not modified. This apparent discrepancy could be attributed to the fact that in our study, AD was maintained for only 48h. The TRPM8 expression was however strongly decreased and we also observed that basal Ca^{2+} influx through the plasma membrane was diminished after AD. This observation could explain the decrease in

$[Ca^{2+}]_{ER}$. Since expression of TRPM8 is known to be dependent of androgen receptor activation [16], we measured basal Ca^{2+} influx after siRNA-mediated TRPM8 depletion. It was decreased in TRPM8-depleted cells suggesting that it was, at least partially, localized in the plasma membrane. However, neither thapsigargin-induced Ca^{2+} release nor SOCE were modified by repression of TRPM8. We therefore conclude that TRPM8 repression and decrease in basal Ca^{2+} influx after AD were not related to the decrease in $[Ca^{2+}]_{ER}$. As expected, AD induced-TRPM8 decrease or siRNA-mediated TRPM8 depletion decreased Ca^{2+} entry. However, they did not modify resting cytosolic $[Ca^{2+}]$, suggesting that their effects on Ca^{2+} entry is compensated by the activity of transporters allowing fluxes of Ca^{2+} out of the cells or into the ER.

As mentioned above, phosphorylated IP3R1 was reported as an ER leak channel in mouse embryonic fibroblasts cells [12]. We therefore measured the expression and the phosphorylation of IP3R1 in AD conditions. Expression was increased by only 50% but phosphorylation on Ser-1716 increased 3-fold after AD for 48h. Inhibiting PKA-dependent phosphorylation of $IP3R1^{S1716}$ by competition with TAT-$IP3R1^{S1716}$ abolished the effect of AD on $[Ca^{2+}]_{ER}$. This underpins the concept that beside its role in response to agonists, IP3R1 also constitutes in LNCaP cells an ER Ca^{2+} leak channel that is modulated by AD-dependent phosphorylation. In those cells, IP3R1 could therefore regulate $[Ca^{2+}]_{ER}$ at rest. Inhibition of PKA by H89 also abolished AD-dependent decrease in $[Ca^{2+}]_{ER}$ but also dramatically increased $[Ca^{2+}]_{ER}$ in the presence of androgen. This could be due to the higher efficiency of H89 to reduce IP3R1 phosphorylation in comparison with TAT-$IP3R1^{S1716}$ (Fig. 5B and D). However, we cannot exclude an alternative pathway connecting PKA and $[Ca^{2+}]_{ER}$.

Our results also clearly show that AD-dependent phosphorylation of IP3R1 is an important mediator of androgen resistance in PCa cells. Indeed, inhibition of IP3R1 phosphorylation with H89 or TAT-$IP3R1^{S1716}$ dramatically increased sensitivity to AD in LNCaP cells. Interestingly, this effect was seriously decreased after pretreatment with thapsigargin, indicating that the effect of PKA on AD-induced cell death is dependent on the Ca^{2+} content in the ER. The role of $[Ca^{2+}]_{ER}$ in

androgen resistance was also confirmed by the fact that SERCA2b overexpression limited the effect of AD on Ca^{2+} store content and increased AD-induced apoptosis. Therefore, we show for the first time that survival of PCa cells in response to androgen removal is dependent on the (partial) depletion of their Ca^{2+} stores.

It has been reported that PKA is overexpressed in PCa and constitutes a marker of poor prognosis [7]. Moreover, PKA hyperactivity could contribute to resistance of PCa cells to AD [29]. Our results suggest that IP3R1 phosphorylation by PKA could explain the decreased AD-induced cell death in HRPCa. Targeting the PKA-IP3R1 pathway could therefore constitute an interesting strategy to restore sensitivity to AD in HRPCa.

Since AD itself induced phosphorylation on the PKA consensus site $IP3R1^{S1716}$, we suggest that, beside its proapoptotic effect, AD concomitantly triggers a prosurvival pathway. Bagchi *et al.* showed that androgen stimulation induced PKA activation by increasing cAMP production [30]. This result is apparently contradictory to our data but it is noteworthy that in contrast to our experimental design (48 h AD), Bagchi *et al.* investigated short-term (10 min) effect of androgen on PKA-related pathways. Furthermore, prolonged AD treatment has been noticed to increase the expression of different catalytic subunits of PKA in LNCaP cells [31].

In a previous study, we showed that AD induced autophagy in LNCaP cells and that this process in turn inhibited AD-triggered cell death [22]. Therefore, we have investigated in the present study whether $IP3R1^{S1716}$ phosphorylation and Ca^{2+} store depletion could be intermediates between AD and autophagy. Our data showed that inhibition of $IP3R1^{S1716}$ phosphorylation does not interfere with AD-induced autophagy. Moreover, siRNA-mediated inhibition of autophagy has no effect on $[Ca^{2+}]_{ER}$. This suggests that AD-induced autophagy and AD-induced $IP3R1^{S1716}$ phosphorylation constitute two independent mechanisms of resistance to AD.

In conclusion, we show that phosphorylation of IP3R1 on a PKA consensus site modulates $[Ca^{2+}]_{ER}$ and renders LNCaP cells more resistant to AD-induced apoptosis. This demonstrates that the

common anti-prostate cancer strategy consisting in androgen removal could interfere with ER Ca^{2+} homeostasis, highlighting the role of ER Ca^{2+} in the mechanisms of cancer aggressiveness.

MATERIALS AND METHODS

Cell culture and reagents

LNCaP cells (American Type Culture Collection, Manassas, VA, USA, CRL-1740) were grown at 37°C in an humidified atmosphere of 5% CO2–95% air in RPMI 1640 (Gibco Invitrogen, Carlsbad, CA, USA, 52400) supplemented with 10% fetal calf serum, 100 IU/ml penicillin (Gibco, 10270) and 100 µg/ml streptomycin (Gibco, 15140). Cells were cultured up to passage 30. Analysis of the effect of androgen deprivation was performed by culturing cells for 2 days in RPMI 1640 medium supplemented with charcoal-treated FCS (Gibco, 12676) for serum steroid hormone removal (-R1881 condition). As control condition, the synthetic agonist of the androgen receptor (AR), methyltrienolone (R1881), was added to the medium at 0.2 nM (+R1881 condition). H89 (Sigma-Aldrich, Saint Louis, MO, B1427) was used at 10 µM, thapsigargin (Sigma-Aldrich, T9033) at 0.5 and 1 µM, ionomycin (Invitrogen, Carlsbad, CA, USA, I24222) at 10 µM. Xestospongin B was purified from Xestospongia exigua as previously described [32]. The synthetic peptide TAT-IP3R1^{S1716} (NH2-RKKRRQRRRGGRPSGRRESLTSFGNG-COOH) was obtained from ThermoFisher Scientific (Waltham, MA, USA) and used at 80 µM.

siRNA transfection

The siRNA targeting TRPM8 mRNA (siTRPM8; 5'-GCAAACUGGUUGCGAACUU-3') as well as the non-silencing control siRNAs (siUNR) pool were purchased from Thermo Fisher Scientific (Lafayette, CO, USA). LNCaP cells were transfected using DharmaFECT reagent (Thermo Fisher Scientific, T-2002-03) according to the manufacturer's instructions. Twenty-four hours later, cells were plated on six-well plates and after 48 additional hours subjected to AD treatment. Four days

after transfection, efficiency of siRNA-mediated depletion of the TRPM8 mRNA was assessed by RT-qPCR.

SERCA2b transfection

LNCaP cells, seeded in six-well culture plates until ~80% confluence, were co-transfected with a plasmid coding a DsRed fluorescent protein and an empty plasmid or a plasmid coding for SERCA2b using Lipofectamine reagent (Invitrogen, 11668-019) according to manufacturer's instructions. After 24 hours, cells were plated on six-well plates and 48 hours later, were subjected to AD treatment during 2 at 3 days.

Quantitative RT-PCR

LNCaP mRNAs were extracted with Trizol reagent (Invitrogen). Gene-specific PCR primers were designed using Primer3 and purchased from Eurogentec (Seraing, Belgium). Primer sequences are given table 1. The β2-microglobulin was used as housekeeping gene. Quantitative RT-PCR was performed using 5 µL of cDNA, 12.5 µL of SYBRGreen Mix (Bio-Rad, Hercules, CA, USA) and 300 nM of each primer in a total reaction volume of 25 µL. The reaction was initiated at 95 °C for 3 min, followed by 40 cycles of denaturation at 95 °C for 10 s, annealing at 60 °C for 1 min, and extension at 72 °C for 10 s. Data were recorded on a MyiQ qPCR detection system (Bio-Rad), and cycle threshold (*Ct*) values for each reaction were determined using analytical software from the same manufacturer. Each cDNA was amplified in duplicate, and *Ct* values were averaged for each duplicate. The average *Ct* value for β2-microglobulin was subtracted from the average *Ct* value for the gene of interest. This Δ*Ct* value obtained in –R1881 condition or in siRNA-TRPM8 silenced LNCaP was then subtracted from the Δ*Ct* value obtained in control conditions (+R1881 or siUNR in +R1881 condition) giving a ΔΔ*Ct* value. As amplification efficiencies of the genes of interest and β2-microglobulin were comparable, the amount of mRNA, normalized to β2-microglobulin, was given by the relation $2^{-\Delta\Delta Ct}$.

Immunoblotting

Cells were harvested by scraping in PBS and re-suspended in lysis buffer containing 20 mM Tris-HCl (pH 7.5), 150 mM NaCl, 1 mM Na_2EDTA, 1 mM EGTA, 1% Triton, 2.5 mM sodium pyrophosphate, 1 mM β-glycerophosphate, 1 mM Na_3VO_4, 1 mM phenylmethanesulfonylfluoride and 1 µg/mL leupeptin. Extracts were diluted in a mix of LDS Sample Buffer and Sample Reducing Agent (NuPAGE®, Invitrogen, NP0007 and NP0009) and heated at 95°C for 3 min. Samples were electrophoresed on 4-12% or 12% SDS-polyacrylamide gels (Invitrogen, NP0321BOX and NP0341BOX) and transferred onto nitrocellulose membranes (Biorad, 162-0097). The blots were saturated in TBS-T buffer (20 mM Tris, 137 mM NaCl, 0.05% Tween 20, pH 7.6) containing 5% skimmed milk for 1 h at room temperature and incubated overnight at 4°C with primary antibodies: anti-TRPM8 (Abcam, Cambridge, UK, ab3243, dilution 1:10,000), and anti-phospho-IP3R^{S1756} (Cell Signaling Technology, Beverly, MA, USA, 3760; recognizing human IP3R1 phosphorylated on Ser-1716), anti-IP3R1 (Cell Signaling Technology, 8568), anti-LC3 (Cell Signaling Technology, 3868) all used at a dilution of 1:1000. Immunodetection of β-actin with monoclonal anti-actin antibody (Sigma-Aldrich, A5441) was used as loading control (dilution 1:10,000). After incubation with appropriate secondary antibodies coupled to peroxidase, peroxidase activity was detected with ECL Prime (GE Healthcare, Uppsala, Sweden, RPN2236) on ECL hyperfilm. Immunoblots were quantified using the *ImageMaster densitometry* program.

Calcium measurements

Cells were plated on glass coverslips, subjected to various treatments during 2 days and then incubated for 1 hour at room temperature with 1 µM Fura-2/AM (Calbiochem, Camarillo, CA, USA) in Krebs-HEPES buffer containing 11.5 mM HEPES, 135.5 mM NaCl, 5.9 mM KCl, 1.8 mM CaCl2, 1.2 mM MgCl2, 11.5 mM D-glucose, pH 7.4. After rinsing, measurements were then realized in Krebs-HEPES buffer without $CaCl_2$ and supplemented with 0.2 mM EGTA. Coverslips were mounted in a heated (37 °C) microscope chamber. Cells were alternately excited (0.5 Hz) at

340 and 380 nm using a Lambda DG-4 Ultra High Speed Wavelength Switcher (Sutter Instrument, Novato, CA, USA) coupled to a Zeiss Axiovert 200 M inverted microscope (Zeiss Belgium, Zaventem, Belgium). Images were acquired with a Zeiss Axiocam camera coupled to a 510-nm emission filter and analyzed with Axiovision software. Cytosolic free Ca^{2+} concentration ($[Ca^{2+}]_c$) was evaluated from the ratio of fluorescence emission intensities excited at the two wavelengths using the Grynkiewicz equation [33].

The progressive fluorescence quenching due to the influx of 100 μM Mn^{2+} (Sigma-Aldrich) was monitored by measurement of Fura-2/AM emission intensity (excitation at 360 nm). The slope of the Mn^{2+}-induced fluorescence quenching was measured on the first 30 seconds after adding Mn^{2+}.

Flow cytometry

Simultaneous detection of mitochondrial membrane potential ($\Delta\Psi_m$) dissipation and plasma membrane permeabilization was determined by staining with 40 nM $\Delta\Psi_m$-sensitive fluorochrome $DiOC_6(3)$ (Molecular Probes-Invitrogen, Carlsbad, CA, USA, D273) and 1 μg/ml vital dye propidium iodide, PI (Sigma-Aldrich, P1304MP). All PI+ events have been considered at DiOC low. Cytofluorometric analyses were performed on a FACSCalibur equipped with CellQuest Pro software (Becton Dickinson, Franklin Lakes, NJ, USA).

GFP-LC3 transfection and imaging

LNCaP cells, seeded in six-well culture plates until ~80% confluence, were transfected with a plasmid coding for GFP-LC3 using Lipofectamine reagent. After 24 hours, cells were plated on glass coverslips and 48 hours later, were subjected to various treatments during 2 days. GFP fluorescence was analyzed on an inverted Axiovert 200 microscope (Zeiss) using FITC excitation and emission wavelengths (100×, NA 1.4, oil immersion). Images were acquired with a Zeiss Axiocam and analyzed by the Zeiss Axiovision software.

Statistical Analysis

Data are presented as means ± SD. Student's t-test and two-way ANOVA were used to determine statistical significance when appropriate.

Acknowledgements

The work was funded by the Belgian agencies "Fonds National de la Recherche Scientifique" and "Fonds de la Recherche Scientifique Médicale", “Fonds Joseph Maisin”, “Télévie”, Concerted Research Action (10-15/029) and the Interuniversity Poles of Attraction Belgian Science Policy (P7/13). D.V. was "Collaborateur Logistique" of the Fund for Medical Scientific Research (FNRS, Belgium) and Chercheur Qualifé (Université catholique de Louvain). GM is a post-doctoral researcher of the FWO. We thank Dr Nadège Zanou and Mrs Valentina Butoescu for helpful comments and technical assistance.

Conflict of interest: The authors declare no competing financial interests.

REFERENCES

[1] N.A. Howlader, A.M. Noone, M. Krapcho, et al., SEER Cancer Statistics Review, 1975-2010 (2013) http://seer.cancer.gov/csr/1975_2010/
[2] D.R. Berthold, G.R. Pond, F. Soban, R. de Wit, M. Eisenberger, I.F. Tannock, Docetaxel plus prednisone or mitoxantrone plus prednisone for advanced prostate cancer: updated survival in the TAX 327 study, J Clin Oncol. 26 (2008) 242-245.
[3] D.P. Petrylak, C.M. Tangen, M.H. Hussain, et al., Docetaxel and estramustine compared with mitoxantrone and prednisone for advanced refractory prostate cancer, N Engl J Med. 351 (2004) 1513-1520.
[4] A. van Bokhoven, M. Varella-Garcia, C. Korch, et al., Molecular characterization of human prostate carcinoma cell lines, Prostate. 57 (2003) 205-225.
[5] J. Connor, I.S. Sawczuk, M.C. Benson, et al., Calcium channel antagonists delay regression of androgen-dependent tissues and suppress gene activity associated with cell death, Prostate. 13 (1988) 119-130.
[6] D.R. Green, G. Kroemer, The pathophysiology of mitochondrial cell death, Science. 305 (2004) 626-629.
[7] C. Giorgi, D. De Stefani, A. Bononi, R. Rizzuto, P. Pinton, Structural and functional link between the mitochondrial network and the endoplasmic reticulum, Int J Biochem Cell Biol. 41 (2009) 1817-1827.

[8] J.P. Decuypere, G. Monaco, G. Bultynck, L. Missiaen, H. De Smedt, J.B. Parys, The IP(3) receptor-mitochondria connection in apoptosis and autophagy, Biochim Biophys Acta. 1813 (2011) 1003-1013.
[9] G. Szabadkai, R. Rizzuto, Participation of endoplasmic reticulum and mitochondrial calcium handling in apoptosis: more than just neighborhood?, FEBS Lett. 567 (2004) 111-115.
[10] C.W. Distelhorst, M.D. Bootman, Bcl-2 interaction with the inositol 1,4,5-trisphosphate receptor: role in Ca(2+) signaling and disease, Cell Calcium. 50 (2011) 234-241.
[11] P. Pinton, C. Giorgi, R. Siviero, E. Zecchini, R. Rizzuto, Calcium and apoptosis: ER-mitochondria Ca2+ transfer in the control of apoptosis, Oncogene. 27 (2008) 6407-6418.
[12] S.A. Oakes, L. Scorrano, J.T. Opferman, et al., Proapoptotic BAX and BAK regulate the type 1 inositol trisphosphate receptor and calcium leak from the endoplasmic reticulum, Proc Natl Acad Sci U S A. 102 (2005) 105-110.
[13] M.J. Chang, F. Zhong, A.R. Lavik, J.B. Parys, M.J. Berridge, C.W. Distelhorst, Feedback regulation mediated by Bcl-2 and DARPP-32 regulates inositol 1,4,5-trisphosphate receptor phosphorylation and promotes cell survival, Proc Natl Acad Sci U S A. 111 (2014) 1186-1191.
[14] S. Bandara, S. Malmersjo, T. Meyer, Regulators of calcium homeostasis identified by inference of kinetic model parameters from live single cells perturbed by siRNA, Sci Signal. 6 (2013) ra56.
[15] S.M. Henshall, D.E. Afar, J. Hiller, et al., Survival analysis of genome-wide gene expression profiles of prostate cancers identifies new prognostic targets of disease relapse, Cancer Res. 63 (2003) 4196-4203.
[16] L. Zhang, G.J. Barritt, Evidence that TRPM8 is an androgen-dependent Ca2+ channel required for the survival of prostate cancer cells, Cancer Res. 64 (2004) 8365-8373.
[17] C. Camello, R. Lomax, O.H. Petersen, A.V. Tepikin, Calcium leak from intracellular stores--the enigma of calcium signalling, Cell Calcium. 32 (2002) 355-361.
[18] V. Vanderheyden, B. Devogelaere, L. Missiaen, H. De Smedt, G. Bultynck, J.B. Parys, Regulation of inositol 1,4,5-trisphosphate-induced Ca2+ release by reversible phosphorylation and dephosphorylation, Biochim Biophys Acta. 1793 (2009) 959-970.
[19] F. Vanden Abeele, L. Lemonnier, S. Thebault, et al., Two types of store-operated Ca2+ channels with different activation modes and molecular origin in LNCaP human prostate cancer epithelial cells, J Biol Chem. 279 (2004) 30326-30337.
[20] S. Nakade, S.K. Rhee, H. Hamanaka, K. Mikoshiba, Cyclic AMP-dependent phosphorylation of an immunoaffinity-purified homotetrameric inositol 1,4,5-trisphosphate receptor (type I) increases Ca2+ flux in reconstituted lipid vesicles, J Biol Chem. 269 (1994) 6735-6742.
[21] T.S. Tang, H. Tu, Z. Wang, I. Bezprozvanny, Modulation of type 1 inositol (1,4,5)-trisphosphate receptor function by protein kinase a and protein phosphatase 1alpha, J Neurosci. 23 (2003) 403-415.
[22] B. Boutin, N. Tajeddine, P. Vandersmissen, et al., Androgen deprivation and androgen receptor competition by bicalutamide induce autophagy of hormone-resistant prostate cancer cells and confer resistance to apoptosis, Prostate. 73 (2013) 1090-1102.
[23] J.P. Decuypere, D. Kindt, T. Luyten, et al., mTOR-Controlled Autophagy Requires Intracellular Ca(2+) Signaling, PLoS One. 8 (2013) e61020.
[24] J.P. Decuypere, K. Welkenhuyzen, T. Luyten, et al., Ins(1,4,5)P3 receptor-mediated Ca2+ signaling and autophagy induction are interrelated, Autophagy. 7 (2011) 1472-1489.
[25] D.J. Klionsky, F.C. Abdalla, H. Abeliovich, et al., Guidelines for the use and interpretation of assays for monitoring autophagy, Autophagy. 8 (2012) 445-544.
[26] A. Bergner, R.M. Huber, Regulation of the endoplasmic reticulum Ca(2+)-store in cancer, Anticancer Agents Med Chem. 8 (2008) 705-709.
[27] H. Akl, G. Bultynck, Altered Ca(2+) signaling in cancer cells: proto-oncogenes and tumor suppressors targeting IP3 receptors, Biochim Biophys Acta. 1835 (2013) 180-193.

[28] K. Vanoverberghe, F. Vanden Abeele, P. Mariot, et al., Ca2+ homeostasis and apoptotic resistance of neuroendocrine-differentiated prostate cancer cells, Cell Death Differ. 11 (2004) 321-330.
[29] D. Merkle, R. Hoffmann, Roles of cAMP and cAMP-dependent protein kinase in the progression of prostate cancer: cross-talk with the androgen receptor, Cell Signal. 23 (2011) 507-515.
[30] G. Bagchi, J. Wu, J. French, J. Kim, N.H. Moniri, Y. Daaka, Androgens transduce the G alphas-mediated activation of protein kinase A in prostate cells, Cancer Res. 68 (2008) 3225-3231.
[31] A.K. Kvissel, H. Ramberg, T. Eide, A. Svindland, B.S. Skalhegg, K.A. Tasken, Androgen dependent regulation of protein kinase A subunits in prostate cancer cells, Cell Signal. 19 (2007) 401-409.
[32] E. Jaimovich, C. Mattei, J.L. Liberona, et al., Xestospongin B, a competitive inhibitor of IP3-mediated Ca2+ signalling in cultured rat myotubes, isolated myonuclei, and neuroblastoma (NG108-15) cells, FEBS Lett. 579 (2005) 2051-2057.
[33] G. Grynkiewicz, M. Poenie, R.Y. Tsien, A new generation of Ca2+ indicators with greatly improved fluorescence properties, J Biol Chem. 260 (1985) 3440-3450.

FIGURE LEGENDS

Figure 1. Intracellular Ca^{2+} homeostasis alterations after androgen deprivation. **(A)** LNCaP cells cultured for 48 h in the presence of 0.2 nM R1881 (+R1881 condition) or in its absence (-R1881 condition) were loaded with Fura-2/AM and stimulated with 1 µM thapsigargin in the absence of extracellular Ca^{2+}. After 5 min, Ca^{2+} was reintroduced in the external medium to evaluate SOCE amplitude. Representative thapsigargin-evoked changes in $[Ca^{2+}]_c$ are presented for both conditions. **(B)** Bar histogram showing in both conditions the $[Ca^{2+}]_c$ measured in Fura-2/AM stained LNCaP cells first in the absence of extracellular Ca^{2+}, then after addition of 1 µM thapsigargin (Thaps) and finally after addition of 1.8 mM extracellular Ca^{2+} (SOCE) (means ± S.D. of five independent experiments, ** $p < 0.01$, *** $p < 0.001$). **(C)** By measurement of Fura-2/AM emission intensity (excitation at 360 nm), the progressive fluorescence quenching due to the influx of Mn^{2+}, taken as a surrogate of Ca^{2+}, was monitored in LNCaP cells in both conditions. The slope of the Mn^{2+}-induced fluorescence quenching was decreased more than twice in the –R1881 condition, revealing that the calcium influx through the cell membrane was strongly decreased after AD (means ± S.D. of three independent experiments).

Figure 2. Bar histogram showing the relative mRNA expression of genes involved in calcium homeostasis after AD in LNCaP cells. Two days after AD treatment, total RNA was extracted and reverse-transcribed. qPCR was performed with specific primers. The mRNA expression of each gene was normalized to β2-microglobulin expression (means ± S.D. of four independent experiments, ** $p < 0.01$, *** $p < 0.001$).

Figure 3. Role of TRPM8 in LNCaP cells. **(A, B)** LNCaP cells were transfected with a siRNA targeting TRPM8 mRNA (siTRPM8) or with a non-silencing control siRNAs (siUNR) pool and then cultured in the presence of 0.2 nM R1881. The silencing of TRPM8 was proved by RT-qPCR (A) and immunoblot (B). β-actin was used as loading control. Four days after transfection, total RNA was extracted and reverse-transcribed. qPCR was performed with specific primers. The results are expressed as the level of TRPM8 expression normalized to β2-microglobulin expression (means ± S.D. of three independent experiments, *** $p < 0.001$). **(B)** Bar histogram showing in siUNR and siTRPM8 conditions the intracellular Ca^{2+} concentrations measured in Fura-2/AM stained LNCaP cells first in the absence of extracellular Ca^{2+} (Rest), then after addition of 1 μM thapsigargin (Thaps) and finally after addition of 1.8 mM extracellular Ca^{2+} (SOCE) (means ± S.D. of three independent experiments). **(C)** Mn^{2+}-induced fluorescence quenching of Fura-2/AM in LNCaP cells four days after transfection with siUNR or siTRPM8 (means ± S.D. of three independent experiments, * $p < 0.05$).

Figure 4. Phosphorylation of IP3R1 on Ser-1716 after AD. **(A)** Immunoblot analysis of the expression of IP3R1 and of its phosphorylation on Ser-1716 in LNCaP cells cultured for 48 h in the presence of 0.2 nM R1881 (+R1881 condition) or in its absence (-R1881 condition). β-actin was used as a loading control. Data presented are representative of seventeen independent experiments. **(B)** Bar histogram showing phosphorylation and total expression level of IP3R1 in both conditions (means ± S.D. of seventeen independent experiments, ** $p < 0.01$, *** $p < 0.001$).

Figure 5. Involvement of IP3R1 phosphorylation in Ca^{2+} homeostasis alterations induced by AD. **(A)** Bar histogram showing the thapsigargin-induced Ca^{2+} release in the absence of extracellular Ca^{2+} measured in Fura-2/AM-loaded LNCaP cells cultured in the presence or in the absence of 0.2 nM R1881 and pretreated or not with 2 μM Xestospongin B (means ± S.D. of three independent experiments, * $p < 0.05$). **(B)** Immunoblot analysis of the expression of IP3R1 and of its phosphorylation on Ser-1716 in LNCaP cells cultured in the presence or in the absence of 0.2 nM R1881 and treated for 48 h with 80 μM cell-permeant TAT-peptide (TAT-IP3R1^{S1716}) containing the Ser-1716 consensus phosphorylation sequence or with 10 μM PKA inhibitor H89 . β-actin was used as a loading control. Data presented are representative of three independent experiments. **(C and D)** Quantification of data presented in A and B (means ± S.D. of three to seven independent experiments, ** $p < 0.01$, *** $p < 0.001$). **(E)** Bar histograms showing the effects of TAT-IP3R1^{S1716} on the $[Ca^{2+}]_c$ measured in Fura-2/AM-loaded LNCaP cells cultured in the presence or in the absence of 0.2 nM R1881 after addition of 10 μM ionomycin in the absence of extracellular Ca^{2+} (means ± S.D. from 6 to 7 independent experiments, * $p < 0.05$). **(F)** Bar histograms showing the effects of H89 on the $[Ca^{2+}]_c$ measured in Fura-2/AM-loaded LNCaP cells cultured in the presence or in the absence of 0.2 nM R1881 after addition of 10 μM ionomycin in the absence of extracellular Ca^{2+} (means ± S.D. from 5 to 6 independent experiments, * $p < 0.05$, *** $p < 0.001$).

Figure 6. Inhibition of IP3R1 phosphorylation sensitizes LNCaP cells to AD. **(A)** Cytofluorimetric assessment of the effects of AD in the absence or in the presence of 80 μM TAT-IP3R1^{S1716} on apoptosis-associated mitochondrial transmembrane potential ($\Delta\Psi_m$) dissipation and plasma membrane permeabilization. Cells were treated for 72 h and then labelled with the $\Delta\Psi_m$-sensitive probe $DiOC_6(3)$ and with propidium iodide (PI). Representative dot plots recorded upon AD treatment in the absence and in the presence of TAT-IP3R1^{S1716} are shown. Numbers in each quadrant indicate the percentage of cells. **(B)** Quantification of data illustrated in A as well as of

cells cultured in the presence of R1881 and similarly treated. White and black columns represent percentages of cells exhibiting $\Delta\Psi_m$ loss alone ($DiOC_6(3)^{low}$) or in association with plasma membrane breakdown (PI+), respectively. Data are presented as means ± S.D. of three independent experiments (* $p < 0.05$). **(C and D)** Similar experiments were performed in the absence or in the presence of 10 µM H89 for 72 h. Effects of thapsigargin (Thaps) were also monitored. Data are presented as means ± S.D. of three independent experiments (* $p < 0.05$, *** $p < 0.001$).

Figure 7. SERCA2b overexpression prevents Ca^{2+} store depletion and promotes cell death after AD. **(A)** LNCaP cells cultured in the presence or in the absence of 0.2 nM R1881 were transfected with a control plasmid or a plasmid encoding SERCA2b and with a dsRed expressing plasmid allowing detection of transfected cells. Cells were loaded with Fura-2/AM and stimulated with 10 µM ionomycin in the absence of extracellular Ca^{2+}. Bar histogram showing the effects of SERCA2b overexpression on the $[Ca^{2+}]_c$ in dsRed-positive cells after addition of ionomycin (means ± S.D. from 4 to 6 independent experiments, *** $p < 0.001$). **(B)** Cytofluorimetric assessment of the effects of AD in dsRed-positive cells on apoptosis-associated mitochondrial transmembrane potential ($\Delta\Psi_m$) dissipation. Transfected LNCaP cells were cultured for 72 h in the presence or in the absence of 0.2 nM R1881 and then labelled with the $\Delta\Psi_m$-sensitive probe $DiOC_6(3)$. Bar histogram shows percentages of dsRed-positive cells exhibiting $\Delta\Psi_m$ loss for each condition. Data are presented as means ± S.D. of three independent experiments (* $p < 0.05$, ** $p < 0.01$).

Figure 8. $[Ca^{2+}]_{ER}$ and autophagy. **(A)** Immunoblot analysis assessing LC3-II protein levels after 48 h AD treatment in with the absence or presence of 10 µM H89. E64d (10 µg/ml) and pepstatin A (10 µg/ml) were added during the treatment. β-actin was used as a loading control. Immunoblots are representative of three independent experiments. **(B)** Quantification of data illustrated in A. Data are presented as means ± S.D. of at least three independent experiments (* $p < 0.05$). **(C)** LNCaP cells were transfected with a plamid encoding a GFP-LC3 fusion protein. Bar histogram showing

the number of cells exhibiting more than 10 fluorescent dots after treatment by 10 μM H89 for 48 h in the presence or in the absence of 0.2 nM R1881 (means ± SD of three independent experiments, ** $p < 0.01$, *** $p < 0.001$). **(D)** LNCaP cells were transfected with a pool of 4 siRNAs targeting Atg5 mRNA (siATG5) or with a non-silencing control siRNAs (siUNR) pool and then cultured in the presence or in the absence of 0.2 nM R1881 for 48 h. LNCaP cells were loaded with Fura-2/AM and stimulated with 1 μM thapsigargin in the absence of extracellular Ca^{2+}. Bar histogram showing thapsigargin-evoked changes in $[Ca^{2+}]_c$ for each condition (means ± S.D. of three independent experiments, *** $p < 0.001$).

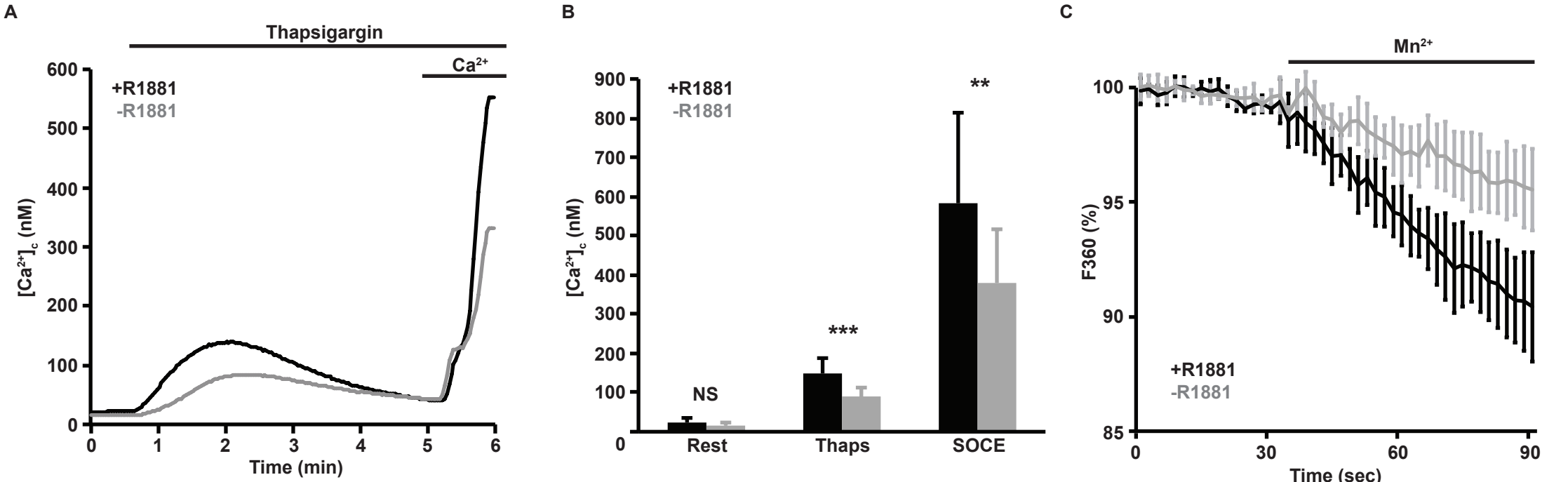
A
Thapsigargin
Ca2+
+R1881
-R1881
[Ca2+]c (nM)
Time (min)
B
+R1881
-R1881
[Ca2+]c (nM)
NS
***
**
Rest
Thaps
SOCE
C
Mn2+
+R1881
-R1881
F360 (%)
Time (sec)

Figure 1

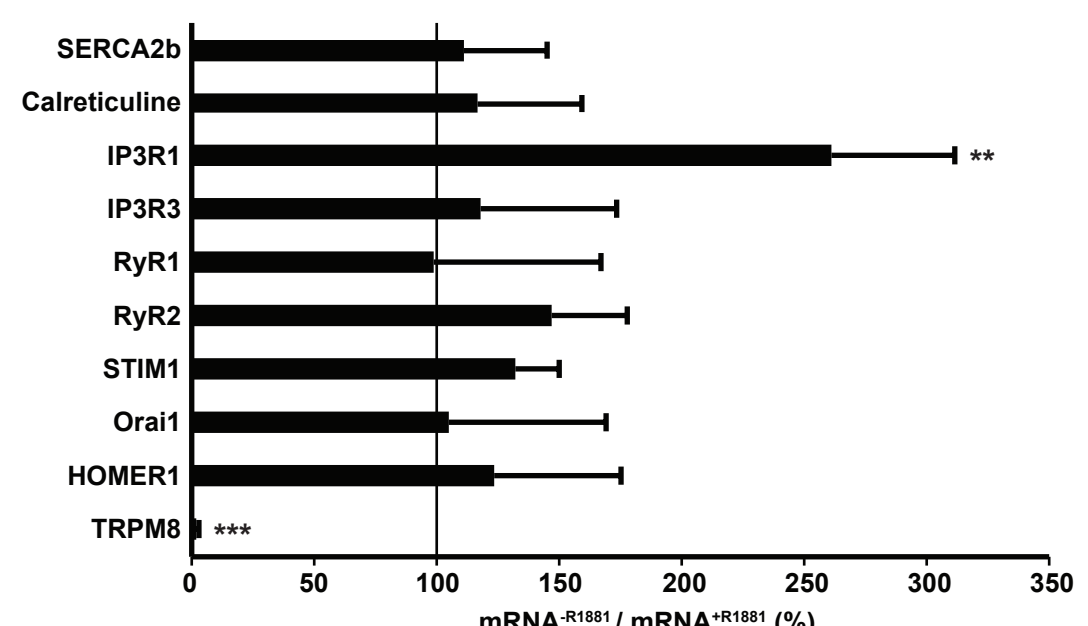
SERCA2b
Calreticuline
IP3R1
**
IP3R3
RyR1
RyR2
STIM1
Orai1
HOMER1
TRPM8
***
0
50
100
150
200
250
300
350
mRNA-R1881 / mRNA+R1881 (%)

Figure 2

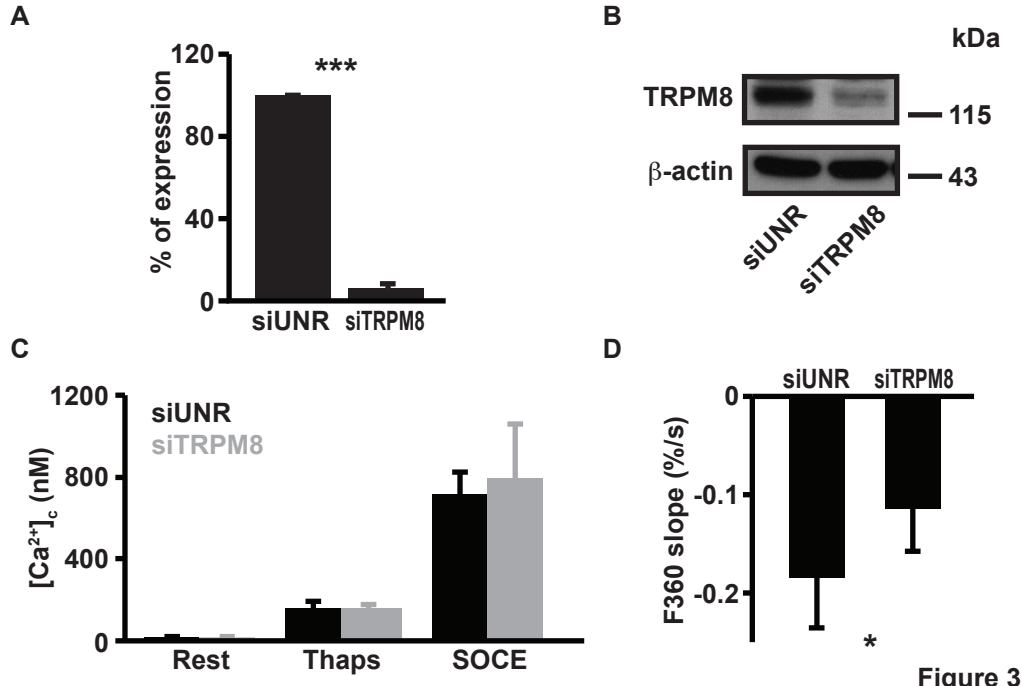
A
120
80
40
0
% of expression
***
siUNR
siTRPM8
B
kDa
TRPM8
115
β-actin
43
siUNR
siTRPM8
C
1200
800
400
0
[Ca2+]c (nM)
siUNR
siTRPM8
Rest
Thaps
SOCE
D
siUNR
siTRPM8
0
-0.1
-0.2
F360 slope (%/s)
*

Figure 3

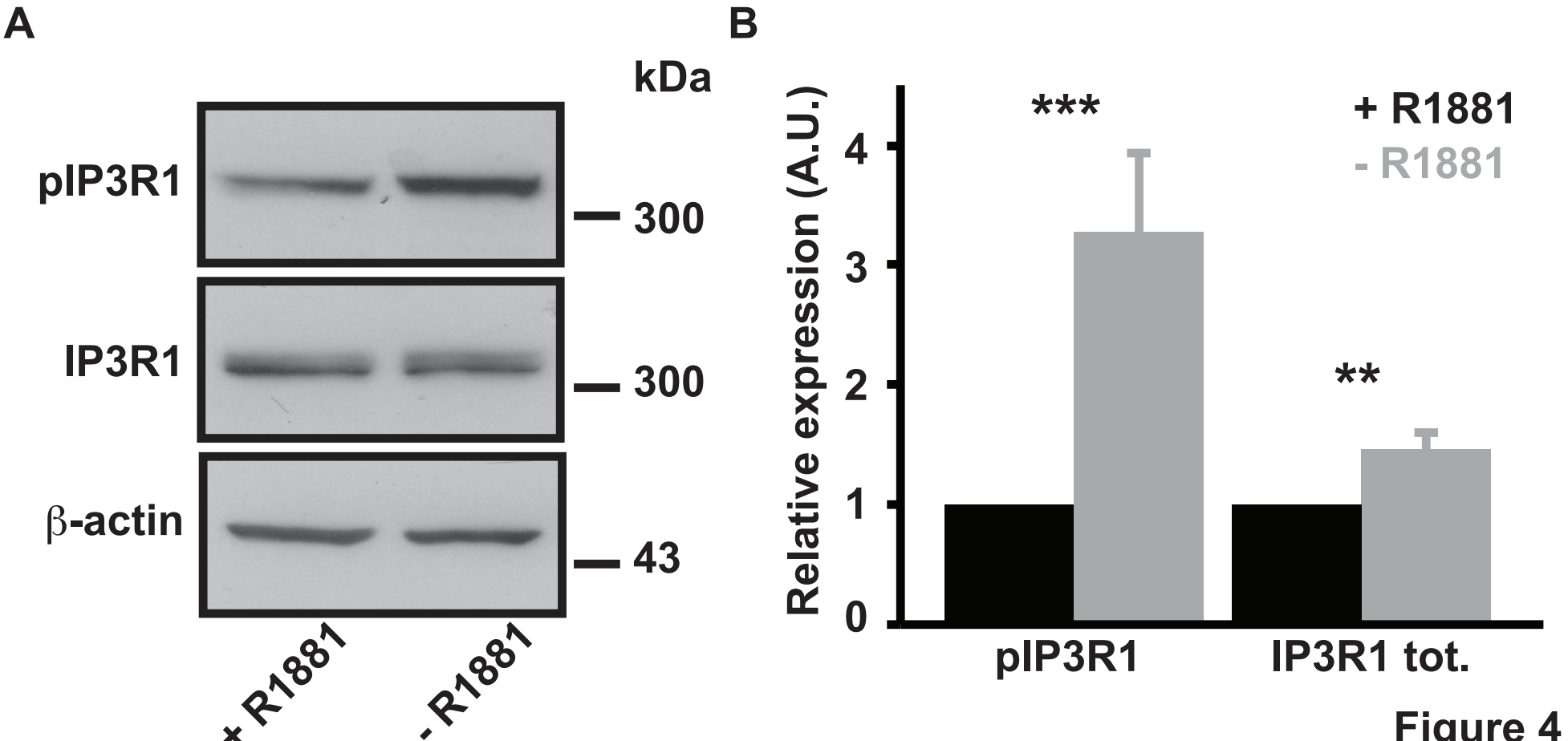
A
kDa
pIP3R1
300
IP3R1
300
β-actin
43
+ R1881
- R1881
B
Relative expression (A.U.)
0
1
2
3
4
***
**
+ R1881
- R1881
pIP3R1
IP3R1 tot.

Figure 4

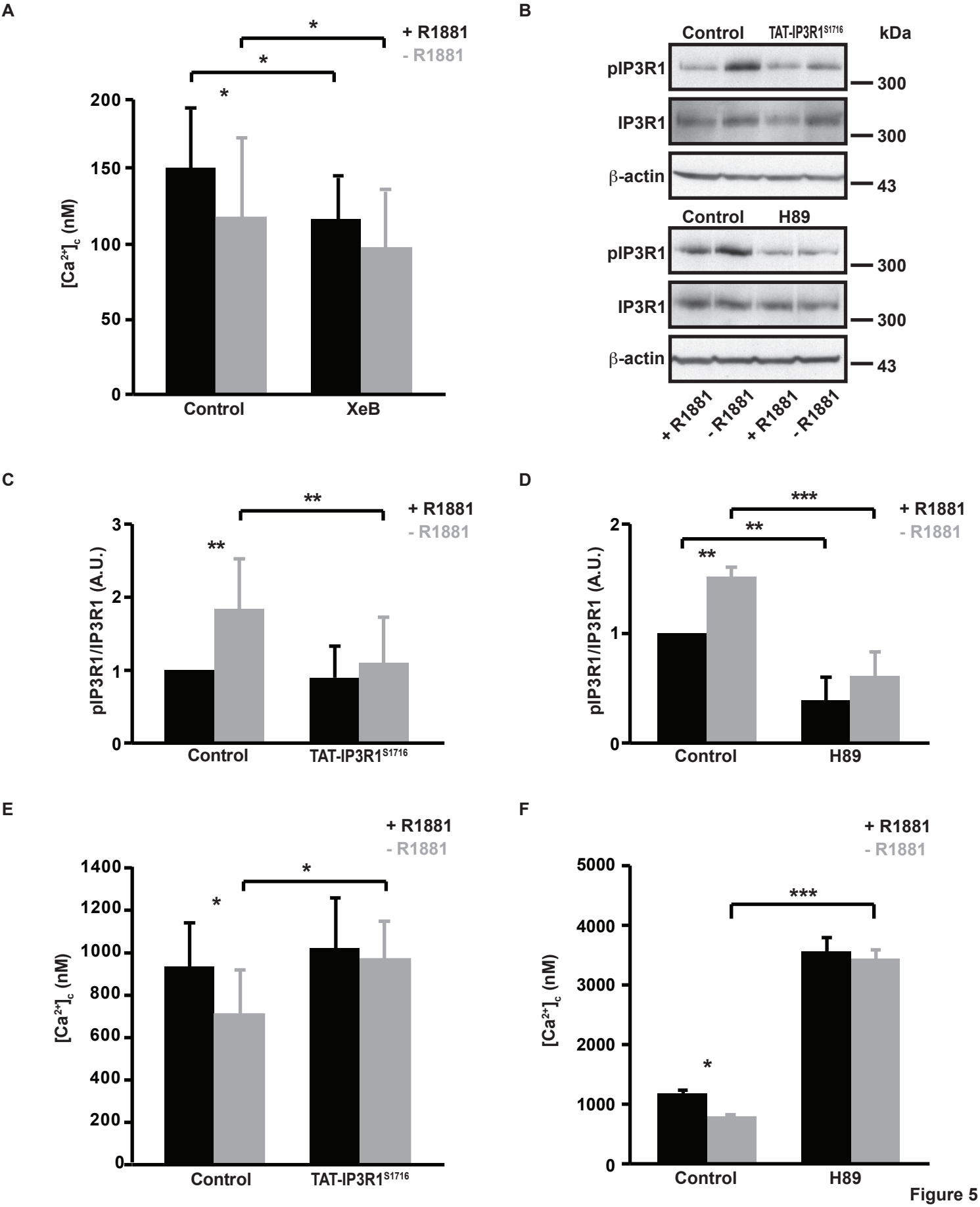
A
+ R1881
- R1881
[Ca2+]c (nM)
Control
XeB
B
Control
TAT-IP3R1S1716
kDa
pIP3R1
IP3R1
β-actin
300
43
Control
H89
+ R1881
- R1881
C
pIP3R1/IP3R1 (A.U.)
Control
TAT-IP3R1S1716
D
H89
E
F

Figure 5

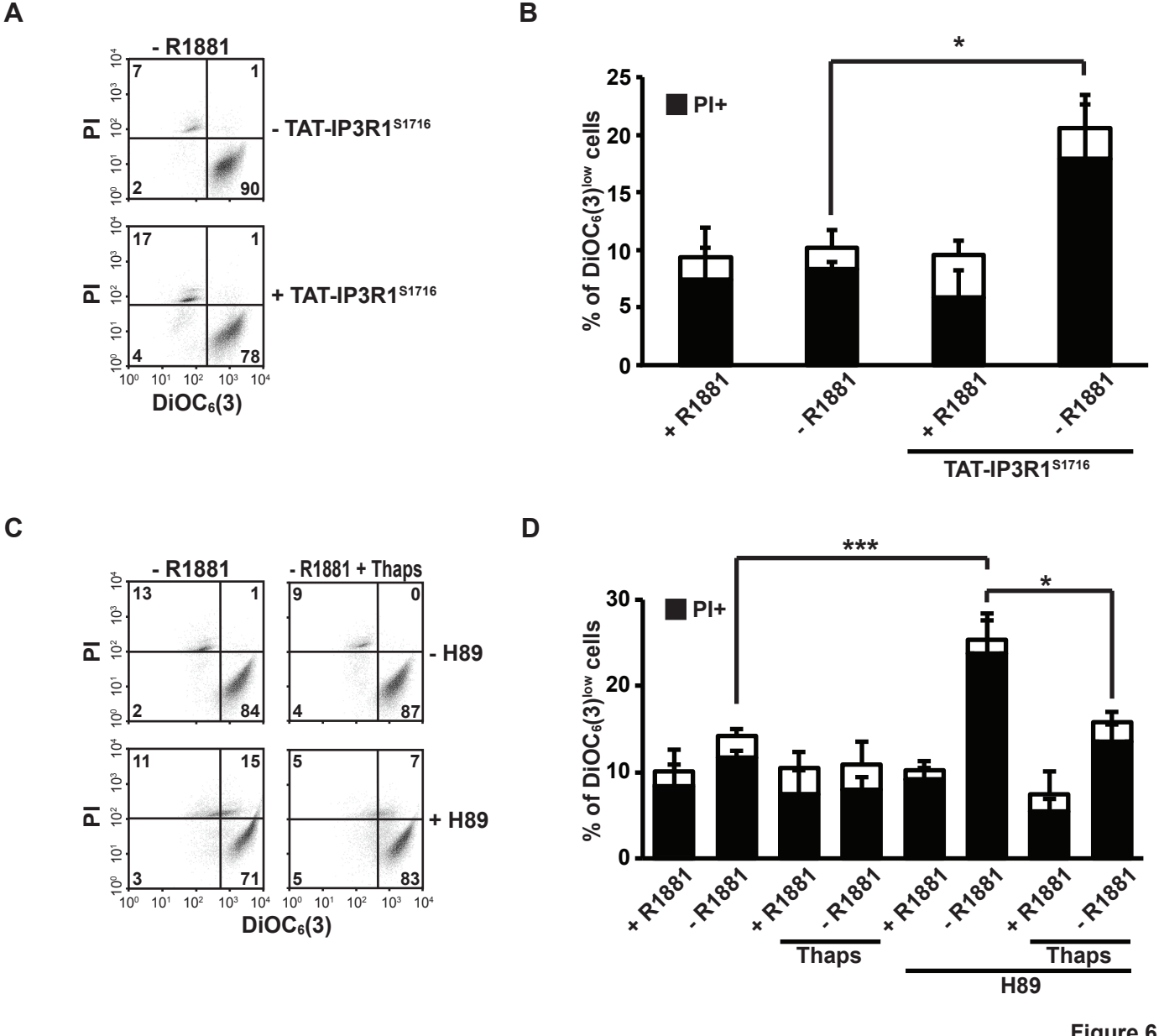
A
- R1881
PI
7
1
2
90
- TAT-IP3R1S1716
17
1
4
78
+ TAT-IP3R1S1716
DiOC6(3)
B
*
PI+
% of DiOC6(3)low cells
+ R1881
- R1881
+ R1881
- R1881
TAT-IP3R1S1716
C
- R1881
- R1881 + Thaps
13
1
2
84
9
0
4
87
- H89
11
15
3
71
5
7
5
83
+ H89
DiOC6(3)
D
***
*
PI+
% of DiOC6(3)low cells
Thaps
Thaps
H89

Figure 6

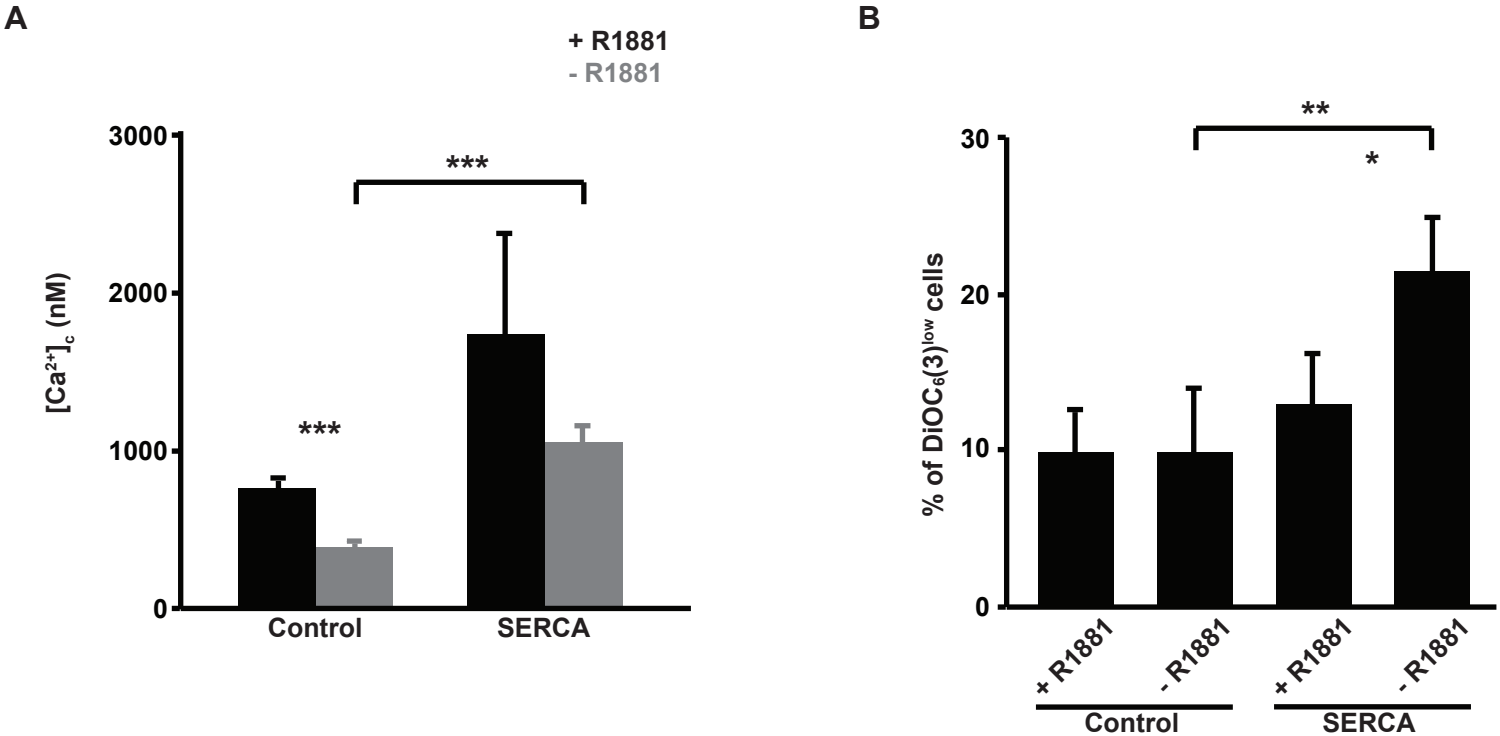
A
+ R1881
- R1881
3000
2000
1000
0
[Ca2+]c (nM)
***
***
Control
SERCA
B
**
*
30
20
10
0
% of DiOC6(3)low cells
+ R1881
- R1881
+ R1881
- R1881
Control
SERCA

Figure 7

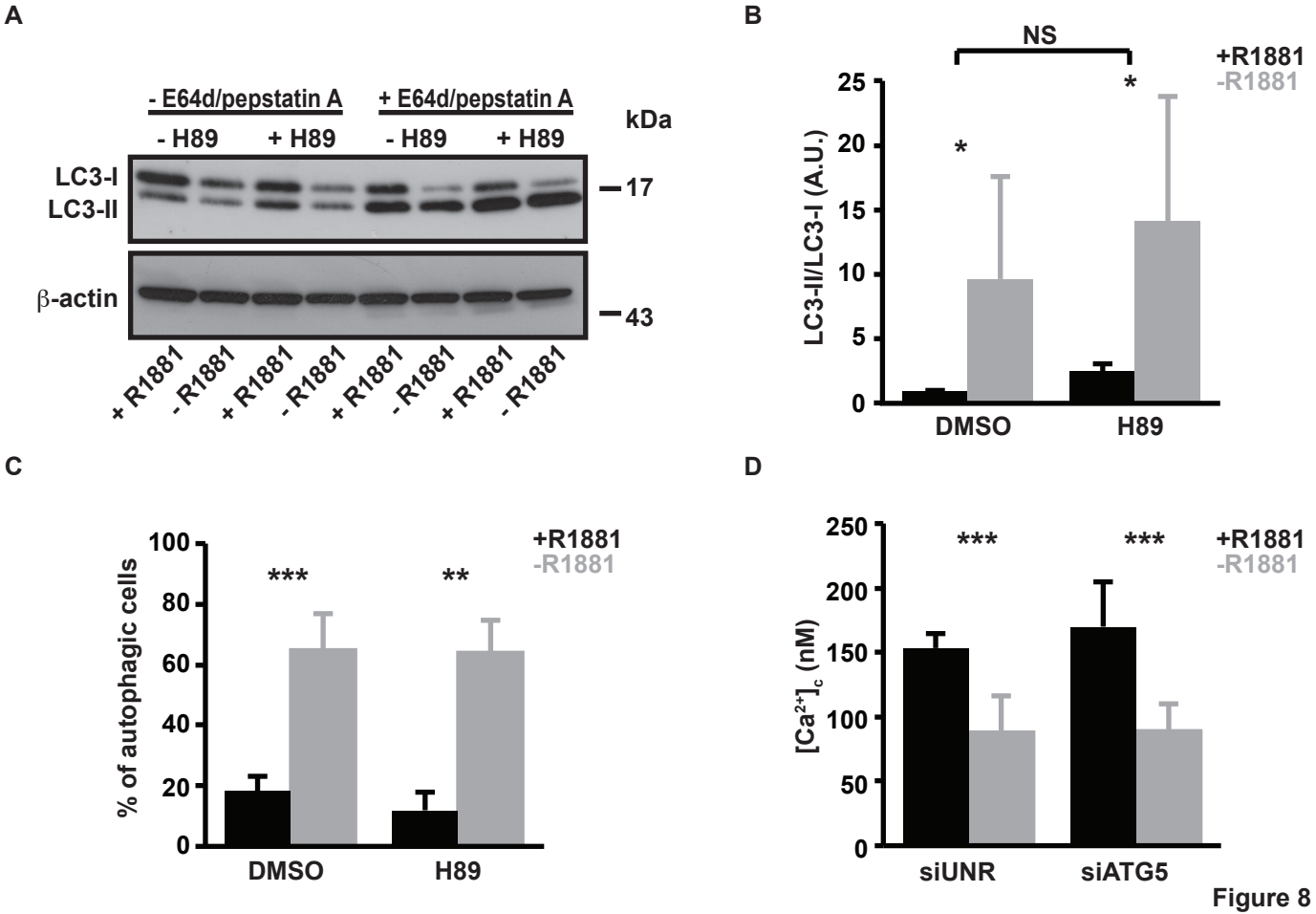
A
- E64d/pepstatin A
+ E64d/pepstatin A
- H89
+ H89
- H89
+ H89
kDa
LC3-I
LC3-II
17
β-actin
43
+ R1881
- R1881
+ R1881
- R1881
+ R1881
- R1881
+ R1881
- R1881
B
NS
+R1881
-R1881
LC3-II/LC3-I (A.U.)
25
20
15
10
5
0
*
*
DMSO
H89
C
+R1881
-R1881
% of autophagic cells
100
80
60
40
20
0
***
**
DMSO
H89
D
+R1881
-R1881
[Ca2+]c (nM)
250
200
150
100
50
0
***
***
siUNR
siATG5

Figure 8